JCI insight

RESEARCH ARTICLE

Sclerostin inhibition alleviates breast cancer–induced bone metastases and muscle weakness

Eric Hesse,[1,2] Saskia Schröder,[1] Diana Brandt,[1] Jenny Pamperin,[1] Hiroaki Saito,[1] and Hanna Taipaleenmäki[1]

[1]Molecular Skeletal Biology Laboratory, Department of Trauma, Hand and Reconstructive Surgery, University Medical Center Hamburg-Eppendorf, Hamburg, Germany. [2]Department of Anatomy and Cell Biology, Indiana University School of Medicine, Indianapolis, Indiana, USA.

Breast cancer bone metastases often cause a debilitating incurable condition with osteolytic lesions, muscle weakness, and a high mortality. Current treatment comprises chemotherapy, irradiation, surgery, and antiresorptive drugs that restrict but do not revert bone destruction. In hormone receptor–negative breast cancer cell lines and human breast cancer tissue, we identified the expression of sclerostin, a soluble Wnt inhibitor that represses osteoblast differentiation and bone formation. In mice with breast cancer bone metastases, pharmacological inhibition of sclerostin using an anti-sclerostin antibody (Scl-Ab) reduced the metastatic burden. Furthermore, sclerostin inhibition prevented cancer-induced bone destruction by augmenting osteoblast-mediated bone formation and by reducing osteoclast-dependent bone resorption. During advanced disease, NF-κB and p38 signaling was increased in muscles in a TGF-β1–dependent manner, causing muscle fiber atrophy, muscle weakness, and tissue regeneration with an increase in Pax7-positive satellite cells. Scl-Ab treatment restored NF-κB and p38 signaling, the abundance of Pax7-positive cells, and muscle function. These effects improved the health and expanded the life span of cancer-bearing mice. Together, these results demonstrate that pharmacological inhibition of sclerostin reduces bone metastatic burden and muscle weakness, with a prolongation of survival time. This might provide novel options for treating musculoskeletal complications in breast cancer patients.

Introduction

Breast cancer is the most common cancer in women worldwide, with prevalence predicted to further increase in the future, representing a tremendous medical and socioeconomic burden (1). After treatment of the primary tumor, metastases often occur years or even decades later (1). Bone is a premier site for breast cancer metastases, and about 70% of breast cancer patients with advanced disease experience osteolytic bone metastases, a stage at which the disease is incurable (2). Osteolytic metastases often cause skeletal-related events (SREs), including pathological fractures and pain, that require palliative interventions (3, 4).

Destruction of the bone tissue in breast cancer–induced osteolytic disease occurs due to an increased number and activity of bone-resorbing osteoclasts (5). Osteoclasts are activated in a direct or indirect manner by cancer- and microenvironment-derived cytokines, including parathyroid hormone–related peptide (PTHrP), receptor activator of NF-κB ligand (RANKL), and interleukins. Upon activation of bone resorption, matrix-derived growth factors and in particular TGF-β further enhance tumor growth and osteoclast activity, constituting a vicious cycle of bone metastasis (5). While it is firmly established that breast cancer cell– and matrix-derived growth factors stimulate osteoclast activity, evidence exists that breast cancer cells also provide molecular cues that suppress osteoblast function (6). Thus, it can be hypothesized that restoring osteoblast function might ameliorate metastatic bone disease. Nevertheless, the exact role of bone-forming osteoblasts in the context of breast cancer metastases–mediated bone destruction and their potential use for pharmacological treatment is not yet elucidated.

In addition to chemotherapy and radiation therapy, patients with osteolytic metastases are treated with antiresorptive drugs such as bisphosphonates or an antibody against RANKL (denosumab; XGEVA, Amgen) that efficiently restrict osteoclast activity and therefore the progression of bone destruction (7).

Conflict of interest: EH and HT are inventors on a patent application (P073406GB) related to this research.

Submitted: October 18, 2018
Accepted: April 2, 2019
Published: May 2, 2019.

Reference information: *JCI Insight*. 2019;4(9):e125543. https://doi.org/10.1172/jci.insight.125543.

Due to advances in surgery, adjuvant chemotherapy, hormone receptor blocking drugs, and antiresorptive therapies, the survival time of patients has been greatly prolonged (8). However, overall morbidity and mortality are still very high, particularly once SREs occur (8). Furthermore, the disease remains irreversible, and osteolytic lesions persist (8).

Since antiresorptive drugs cannot revert osteolytic lesions, augmenting osteoblast function has been proposed as a potential approach to restore bone integrity in the context of metastasis-induced osteolytic lesions (9). To date, only 2 bone anabolic drugs are available in the clinic for the treatment of osteoporosis, a debilitating disease that leads to loss of bone mass and ultimately fragility fractures. Intermittent administration of a recombinant fragment of parathyroid hormone (PTH 1-34; teriparatide; Forteo/Forsteo, Eli Lilly and Co.) or of a PTH-related peptide analog (PTHrP 1-34; abaloparatide; Tymlos, Radius) increase osteoblast-mediated bone formation and bone mass but are not approved for use in cancer patients (6). Thus, there is currently no osteoblast-targeting drug available that could be used for the treatment of cancer-related bone disease.

Osteoblast differentiation and function is regulated by a network of transcription factors and signaling pathways (10). Canonical Wnt signaling is among the most prominent pathways promoting osteoblast differentiation, function, and bone formation (11). Activation of the canonical Wnt pathway occurs upon binding of Wnt ligands to low-density lipoprotein receptor–related proteins 5 and 6 (Lrp5/6), which form a complex with frizzled-related proteins. Sclerostin is a soluble Wnt antagonist that prevents binding of Wnt ligands to Lrp5/6 and therefore the activation of the pathway and ultimately osteoblast-mediated bone formation (11). Due to its strong inhibitory effect on Wnt signaling and pharmacological accessibility, sclerostin has emerged as a promising drug target, and anti-sclerostin antibodies (Scl-Ab) have been developed to increase bone formation and bone mineral density (BMD) in the context of postmenopausal osteoporosis (12, 13). In clinical trials, treatment of women with postmenopausal osteoporosis with Scl-Ab (romosozumab; Evenity, Amgen/UCB) increased bone formation, while bone resorption was decreased, leading to an increase in BMD and a reduction of the fracture rate at several sites, including the hip and spine (13, 14). Recently, romosozumab was approved in Japan and in the United States for the treatment of severe postmenopausal osteoporosis, and it is expected to become available in the Europe later in 2019. Thus far, activation of the canonical Wnt signaling pathway in the skeleton has not caused any malignant side effect, either in preclinical animal models or by genetic or pharmacological means in humans, demonstrating the overall safety of this approach in the musculoskeletal system. The strong effect of Wnt activation on increasing BMD and decreasing the fracture rate is also of interest in the context of bone fragility syndromes other than osteoporosis. For instance, osteogenesis imperfecta (OI) is often caused by mutations in the gene encoding collagen type 1, leading to brittle bones and fractures (15). In this context, another Scl-Ab (BPS-804, setrusumab; Mereo BioPharma) is currently being investigated in clinical trials for the treatment of patients with OI (16).

In breast cancer patients, SREs are often associated with muscle weakness, a debilitating condition that decreases mobility, well-being, and life quality of breast cancer patients (17, 18). The disease mechanisms underlying cancer-associated muscle weakness are largely unknown, and no therapy is available to date (17, 18). Thus, novel therapeutic approaches targeting breast cancer bone metastases and muscle weakness are urgently needed.

Here we report that metastatic breast cancer cells secrete sclerostin, thereby inhibiting canonical Wnt signaling in osteoblasts and osteoblast differentiation, indicating that breast cancer cells might impair bone formation while promoting metastases and bone resorption. Treatment of bone metastases–bearing female mice with Scl-Ab (setrusumab) alleviated tumor growth in bone and bone destruction without increasing metastases at other sites. Surprisingly, Scl-Ab treatment protected from cancer-induced muscle fiber atrophy and loss of muscle function in tumor-bearing mice and prolonged the life span of these animals. These findings reveal that therapeutic inhibition of sclerostin reduces breast cancer-induced bone metastases and muscle weakness in mice, indicating its potential as a novel therapeutic option for breast cancer patients.

Results

Breast cancer cell–derived sclerostin inhibits Wnt signaling in osteoblasts. To address the hypothesis that metastatic breast cancer cells impair osteoblast differentiation, we collected conditioned medium from MDA-MB-231 metastatic breast cancer cells and differentiated primary calvarial cells into osteoblasts in the presence or absence of medium that had been conditioned by breast cancer cells. In support of our hypothesis, conditioned medium inhibited osteoblast differentiation and matrix mineralization, demonstrated by reduced

expression of the osteoblast marker genes *Runx2* and *Ocn* and weaker alizarin red S staining (Figure 1, A and B). Furthermore, using a TOPflash reporter gene assay, we determined that cancer cell–conditioned medium suppressed the activity of the canonical Wnt signaling pathway in osteoblasts in a dose-dependent manner (Figure 1C). These findings indicate that metastatic breast cancer cells may secrete factors that inhibit canonical Wnt signaling in osteoblasts in a paracrine fashion.

Breast cancer cells have been shown to express Dickkopf 1 (Dkk1), a soluble antagonist of canonical Wnt signaling. However, antagonizing cancer cell–derived Dkk1 did not fully restore the activity of the Wnt pathway (19), suggesting that additional mechanisms might exist. Indeed, expression analysis revealed significantly higher expression of the Wnt inhibitor sclerostin in metastatic MDA-MB-231 breast cancer cells compared with nonmetastatic MCF-7 breast cancer cells (Figure 1D). To determine whether sclerostin expression is a general feature of breast cancer cells, we performed an in silico analysis using the EMBL-EBI Expression Atlas (20). In addition to cells of the MDA-MB-231 cell line, expression of sclerostin was found in cells of the SUM159PT, CAL51, HCC 1187, HCC 1197, HCC 1395, HCC 1806, and KPL-4 breast cancer cell lines. Interestingly, 6 of these cell lines (SUM159PT, CAL51, HCC 1187, HCC 1197, HCC 1395, and HCC 1806) express neither the estrogen receptor (ER) nor the progesterone receptor (PR) and do not bear an amplification of the HER-2/Neu gene (referred to as triple-negative breast cancer cells) (21, 22). Furthermore, although KPL-4 cells have a HER-2/Neu amplification, they do not express the ER or the PR (23), suggesting that sclerostin expression is a common feature of hormone receptor–negative breast cancer cells. To address the question of whether sclerostin is expressed in primary breast cancer tissue from patients, we quantified sclerostin expression in tissue biopsies obtained from 48 breast cancer patients and from 4 healthy individuals. While sclerostin expression was not detected in healthy breast tissue, 21% of primary breast cancers expressed sclerostin (Figure 1E). Interestingly, 56% of triple-negative breast cancer tissues and 43% of ER-negative and PR-negative breast cancer tissues expressed sclerostin (Figure 1E). Furthermore, 2 of 3 (66 %) metastatic breast cancers with unknown receptor status were positive for sclerostin expression. Tumors expressing either the ER or the PR or both receptors did not express sclerostin (data not shown). To determine whether sclerostin expression is a specific feature of breast cancer or if it is also expressed by other types of cancer, we analyzed sclerostin expression in human colon (n = 9), kidney (n = 9), liver (n = 9), lung (n = 9), prostate (n = 9), ovary (n = 9), and thyroid (n = 9) cancer biopsies and the respective healthy tissue. Sclerostin expression was detected in 2 colon (22%), 1 ovary (11%), and 2 lung (22%) cancer tissues, suggesting that although sclerostin expression is not specific to breast cancer, it is not a general oncogenic feature of all types of cancer (Table 1).

To investigate whether breast cancer cell–derived sclerostin reduces Wnt signaling activity in osteoblasts, we restricted sclerostin expression in MDA-MB-231 cells using 3 different siRNAs designed to target *SOST* mRNA (Supplemental Figure 1, A and B). Next, conditioned medium was obtained from MDA-MB-231 cells transfected with scrambled control siRNA or siRNA targeting *SOST* mRNA. Indeed, antagonizing sclerostin expression in metastatic breast cancer cells partially but significantly restored the impaired Wnt signaling activity in calvarial osteoblasts (Figure 1F).

Sclerostin inhibits the activation of the canonical Wnt signaling pathway in osteoblasts by binding to the first β-propeller domain of the extracellular region of the LRP5 receptor (24). Heterozygous missense mutations (G171V and A214V) within this domain of LRP5 cause a high bone mass phenotype in patients and in mice due to reduced binding of sclerostin (25, 26). To determine whether cancer cell–derived sclerostin inhibits Wnt activity in osteoblasts through Lrp5, we obtained osteoblasts from genetically modified mice heterozygous for the *Lrp5* mutation G171V. In support of our hypothesis, osteoblasts bearing a mutant *Lrp5* with a disabled sclerostin binding site were resistant to breast cancer–mediated repression of Wnt signaling (Figure 1G). These data suggest that breast cancer cells impair osteoblast differentiation, at least in part, by a sclerostin/Lrp5-mediated inhibition of the canonical Wnt signaling pathway.

Pharmacological inhibition of sclerostin reduces bone metastatic burden and prolongs survival time. Given the negative effect of cancer-derived sclerostin on osteoblasts, we hypothesized that inhibition of sclerostin and subsequent activation of osteoblast function might protect from the progression of metastatic bone disease. To investigate the therapeutic potential of Scl-Ab treatment in breast cancer–induced bone destruction, an in vivo metastasis model was used in which MDA-MB-231 breast cancer cells stably expressing the luciferase gene (MDA-MB-231-*luc*) were inoculated by cardiac injection into 8-week-old female SCID mice. To recapitulate the clinical situation of breast cancer patients, bone metastases were allowed to form in mice prior to treatment. Two weeks after breast cancer cell injection, micrometastases

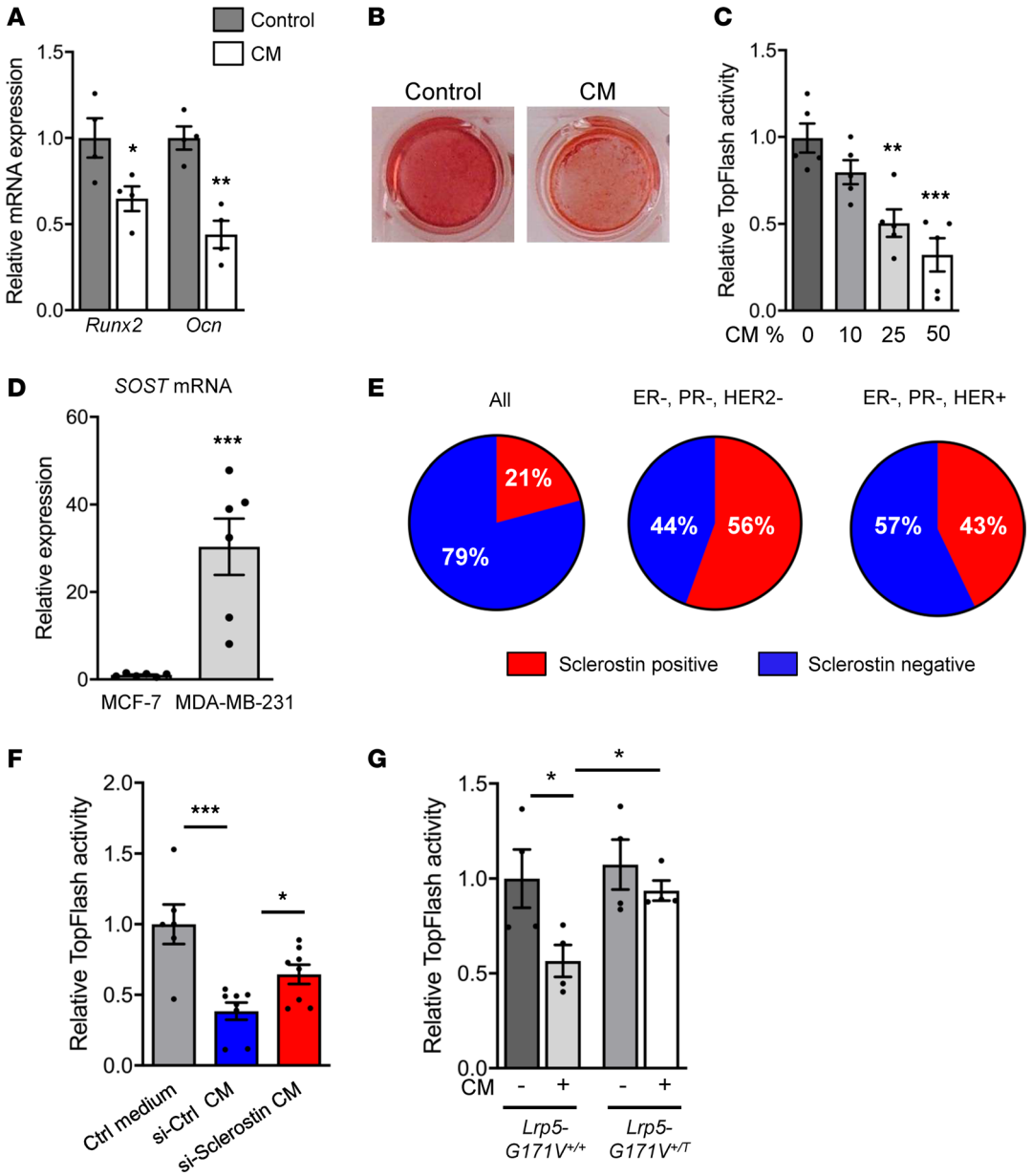

Figure 1. Breast cancer–derived sclerostin inhibits Wnt signaling in osteoblasts. (**A** and **B**) Calvarial cells were differentiated into osteoblasts in the presence of control medium or cancer-conditioned medium (CM) collected from MDA-MB-231 metastatic breast cancer cells. Osteoblast differentiation was determined by quantification of *Runx2* and osteocalcin (*Ocn*) gene expression (**A**) and by alizarin red S staining (**B**) (n = 4 independent experiments). (**C**) Calvarial osteoblasts were cultured in the presence of the indicated amount of MDA-MB-231–derived CM. Wnt signaling activity was determined by TOPflash reporter assay (n = 4 independent experiments). (**D**) Sclerostin mRNA expression was quantified in nonmetastatic MCF-7 and metastatic MDA-MB-231 breast cancer cells by qRT-PCR (n = 6 independent experiments). (**E**) *SOST* mRNA expression was analyzed in breast cancer tissue from 48 patients. Proportion of sclerostin-positive and sclerostin-negative tissue samples is shown for all patients and for triple-negative (ER–, PR–, HER–) and in hormone receptor–negative (ER–, PR–, HER+) patients. All, n = 48; ER–, PR–, HER-, n = 9; ER–, HER–, HER+, n = 7. (**F**) Wnt signaling activity in calvarial osteoblasts cultured with control medium or with CM from MDA-MB-231 cells transfected with scrambled control siRNA (si-Ctrl CM) or siRNA against sclerostin (si-Sclerostin CM) (n = 6 independent experiments). (**G**) Wnt signaling activity in calvarial osteoblasts isolated from mice heterozygous for the *Lrp5* mutation G171V (*Lrp5-G171V*$^{+/T}$) and from control littermates (*Lrp5-G171V*$^{+/+}$) stimulated with control medium or cancer CM (n = 4 independent experiments). Data are presented as mean ± SEM. Two-tailed Student's t test was used to compare 2 groups (**A** and **D**), and ANOVA followed by Tukey's post hoc analysis was used to compare 3 or more groups (**C**, **F**, and **G**); $^*P < 0.05$, $^{**}P < 0.01$, $^{***}P < 0.001$.

Table 1. Sclerostin expression in different cancers

Cancer type	Total number	Sclerostin-positive	Sclerostin-negative
Adenocarcinoma of colon	9	2 (22 %)	7 (78%)
Carcinoma of kidney, renal cell	9	0	9 (100%)
Carcinoma of liver (all)	9	0	9 (100%)
Hepatocellular	8	0	8
Cholangiocarcinoma of liver	1	0	1
Carcinoma of lung (all)	9	2 (22%)	7 (78%)
Adenocarcinoma of lung	2	0	2
Squamous cell carcinoma	5	1	4
Non-small cell carcinoma	2	1	1
Ovary cancer (all)	9	1 (11%)	8 (89%)
Tumor of ovary, borderline	2	0	2
Adenocarcinoma of ovary	7	1	6
Prostate (all)	9	0	9 (100%)
Hyperplasia of prostate	6	0	6
Prostatitis	2	0	2
Adenocarcinoma of prostate	1	0	1
Carcinoma of thyroid	9	0	9 (100%)

were detected in the long bones by bioluminescence imaging, and mice were randomized into 2 treatment arms. One group was treated with Scl-Ab (100 mg/kg), while the other group received vehicle control (50 μl/10g) i.v. once a week for 4 weeks. Non-cancer-bearing mice without treatment, or with vehicle or Scl-Ab treatment served as healthy controls. Weekly bioluminescence imaging of cancer-bearing mice revealed progressive growth of bone metastases in vehicle-treated mice (Figure 2, A and B). Although metastases also developed in mice that received Scl-Ab, tumor growth in bones was significantly reduced compared with vehicle-treated controls (Figure 2, A and B). The reduced tumor growth was confirmed by histological analyses of metastasis area in tibiae (Figure 2, C and D) and in the femur (Supplemental Figure 2A) of cancer-bearing mice. To evaluate the potential effects of Scl-Ab treatment on cancer cell relocation and metastasis formation at other sites, several organs including lung, liver, and brain were imaged by ex vivo bioluminescence after sacrifice (data not shown). Furthermore, expression of HLA was determined by quantitative PCR (qRT-PCR) and immunohistochemistry in the brain and lung, which are the most common sites of breast cancer metastases after bone. Importantly, inhibition of sclerostin did not change the abundance of breast cancer cells at extraskeletal sites such as lung and brain (Figure 2, E and F, and Supplemental Figure 2B), indicating that Scl-Ab treatment of mice with bone metastases does not cause breast cancer cell dissemination into other organs. Due to the strong reduction of bone metastatic burden, we hypothesized that Scl-Ab treatment might be beneficial for the overall life span. Indeed, Scl-Ab treatment significantly prolonged the survival time of breast cancer–bearing mice (Figure 2G).

Sclerostin antibody treatment protects from breast cancer–induced bone destruction. To test the hypothesis that inhibition of sclerostin might be a therapeutic approach to prevent bone destruction or to restore bone integrity in the context of breast cancer-mediated bone destruction, bone mass of mice with and without bone metastases was quantified by microcomputed tomography (μCT). Consistent with previous reports (27), Scl-Ab treatment of non-tumor-bearing mice increased trabecular bone mass of the distal femur (Supplemental Figure 3, A and B) and of the proximal tibia (Supplemental Figure 3, C and D), as well as cortical thickness of the femur midshaft (Supplemental Figure 3, E and F). In mice with bone metastases, Scl-Ab treatment protected from breast cancer–induced osteolytic lesions and subsequent loss of bone mass of the distal femur (Figure 3A) and of the proximal tibia (Figure 3B). Furthermore, histological analyses of the proximal tibia revealed a significantly reduced bone formation rate and bone mass in cancer-bearing vehicle-treated mice compared with healthy vehicle-treated control animals (Figure 3, C–E). Intriguingly, Scl-Ab treatment of mice with bone metastases increased both bone mass and bone formation to the level of healthy Scl-Ab–treated mice (Figure 3, D and E). Detailed histomorphometric analysis of the bone surfaces nearby metastases revealed that the presence

of breast cancer cells blunted bone formation in vehicle-treated mice, which was significantly restored by Scl-Ab treatment (Figure 3, F and G). These results suggest that Scl-Ab prevents bone loss in the context of bone metastases at least in part by restoring breast cancer–inhibited bone formation at the bone-tumor interface.

To further analyze the mode of action of Scl-Ab in mice with breast cancer bone metastases, amino propeptide of type I collagen (P1NP) and tartrate-resistant acid phosphatase 5b (TRAP5b) were measured in the serum of cancer-bearing mice as biomarkers for bone formation and bone resorption, respectively. While the P1NP serum concentration was higher in Scl-Ab–treated mice, the serum concentration of TRAP5b was decreased compared with vehicle-treated animals, suggesting that Scl-Ab treatment activates bone formation and reduces bone resorption (Supplemental Figure 4, A and B). This dual mode of action has been consistently reported in the context of the treatment of postmenopausal osteoporosis (13, 14). To further investigate this finding at a cellular level, parameters of osteoblasts and osteoclasts were quantified in cancer-bearing mice. As expected, the number and size of bone-forming osteoblasts were significantly increased in Scl-Ab–treated cancer-bearing mice compared with vehicle-treated control animals (Figure 3, H and I). Furthermore, the number and size of bone-resorbing osteoclasts were strongly reduced in response to Scl-Ab treatment (Figure 3, J and K, and Supplemental Figure 4C), suggesting that the increase in bone mass was due to a concomitant increase in bone formation and a reduction in bone resorption. Together, these data strongly indicate that Scl-Ab treatment not only increases bone mass through its anabolic action by restoring the tumor-induced impairment of osteoblast function, but also reduces the breast cancer–mediated increase in osteoclast activity, thereby reverting osteolytic disease.

Inhibition of sclerostin prevents breast cancer–induced loss of muscle function. Patients with bone metastases often experience muscle weakness (17, 18). Similarly, mice with breast cancer–induced metastatic bone disease have a reduced ex vivo muscle contractility compared with healthy animals (Figure 4A) (17). Given the beneficial effect of Scl-Ab in reducing tumor burden and bone destruction, we postulated that inhibition of sclerostin might also affect muscle function. To test this hypothesis, we analyzed the specific muscle force and endurance of the extensor digitorum longus (EDL) muscles of healthy mice and of mice with bone metastases treated with Scl-Ab or vehicle control. Although Scl-Ab treatment increased bone mass in healthy mice (Figure 3, C and D, and Supplemental Figure 3), muscle function was not altered in these animals (Figure 4A). In contrast, Scl-Ab treatment of mice bearing bone metastases protected from cancer-induced muscle weakness, as determined by quantification of specific muscle force (Figure 4A) and endurance (Figure 4B). To better understand the disease mechanism of the altered muscle function, tibialis anterior (TA) muscles were stained for succinate dehydrogenase and the cross-sectional area (CSA) of oxidative and nonoxidative fibers was quantified. Consistent with an unchanged muscle function, Scl-Ab treatment of healthy mice did not affect the CSA of either oxidative nor nonoxidative muscle fibers (Figure 4, C and D). Interestingly, bone metastases caused a significant reduction in CSA, which was fully restored by Scl-Ab treatment (Figure 4, C and D). Since oxidative muscle fibers were affected in cancer-bearing mice (Figure 4D), it appears likely that metastatic bone disease may cause oxidative stress and muscle fiber atrophy in skeletal muscles, which is prevented by treatment with Scl-Ab.

Antagonizing sclerostin reverses breast cancer–induced increase in NF-κB signaling. To further elucidate the molecular mechanisms underlying the effect of Scl-Ab on skeletal muscles of cancer-bearing mice, we investigated various signaling pathways involved in oxidative stress. Western blot analysis revealed increased phosphorylation of p38, ERK1/2, and STAT3 in gastrocnemius (GAS) muscle of cancer-bearing mice compared with healthy control animals (Figure 5A and Supplemental Figure 5A). Interestingly, the cancer-induced phosphorylation of p38 was reversed in the muscles of Scl-Ab–treated animals (Figure 5A). Since activation of the NF-κB pathway has been shown to be a critical component of skeletal muscle atrophy (28), we investigated whether NF-κB signaling is also implicated in breast cancer–induced bone metastases. Under steady-state conditions, NF-κB is sequestered in the cytoplasm through interaction with members of the inhibitor of κB (IκB) family of proteins. Upon activation, the IKK complex, which contains the IκB kinases IKKα and IKKβ, phosphorylates the IκB proteins, thereby targeting them to ubiquitination and proteasomal degradation (28). Interestingly, IKKα and IKKβ were strongly phosphorylated in the muscles of cancer-bearing mice treated with vehicle compared with healthy animals. Furthermore, phosphorylation of the NF-κB subunit p65 was strongly increased in cancer-bearing mice, indicating activated NF-κB signaling. Phosphorylation of IKKα, IKKβ, and p65

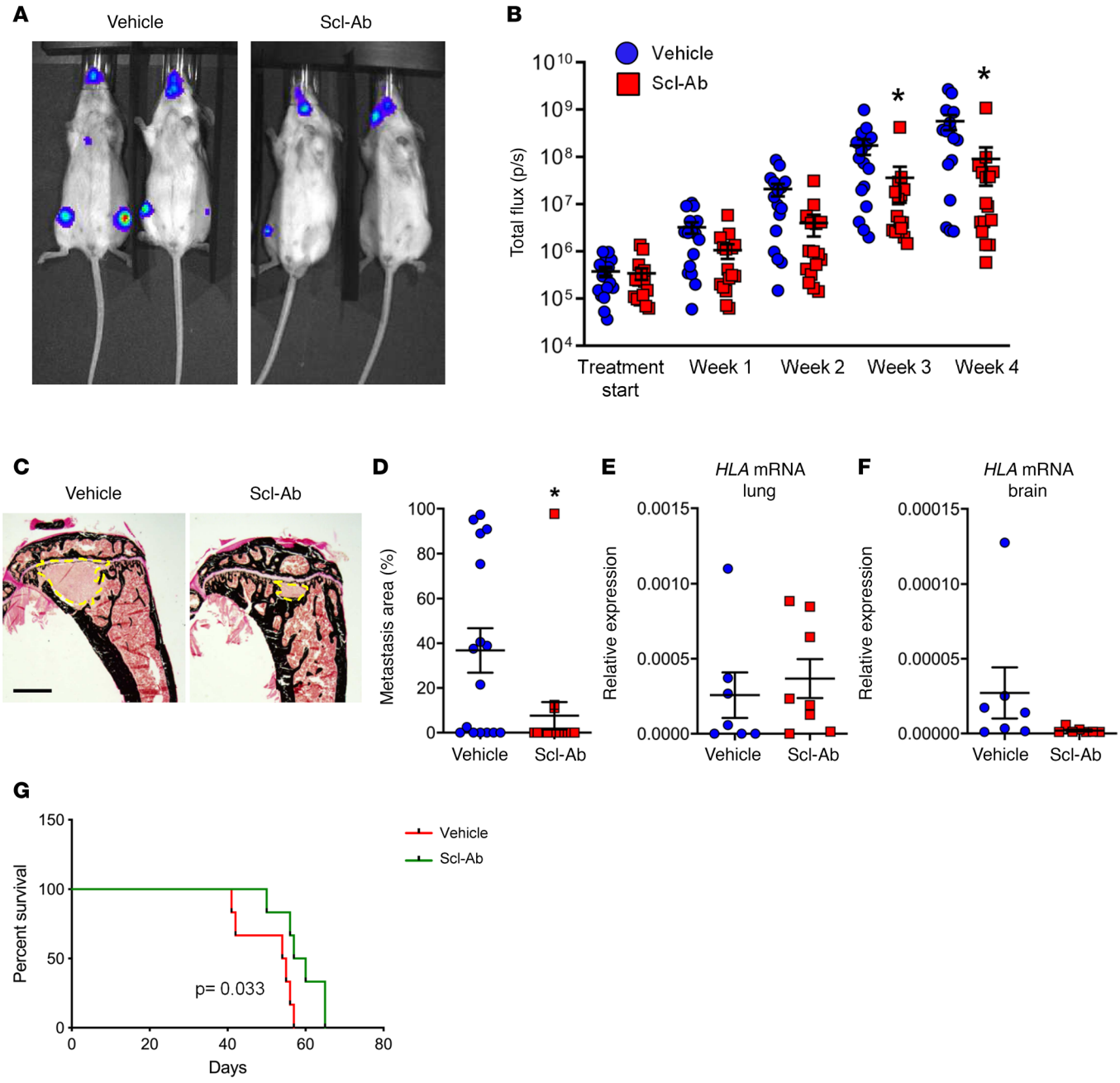

Figure 2. Pharmacological inhibition of sclerostin reduces bone metastatic burden in mice. MDA-MB-231 breast cancer cells stably expressing the luciferase gene were injected into the left ventricle of 8-week-old female immune-compromised SCID mice. Micrometastases were detected 2 weeks after breast cancer cell injection by bioluminescence imaging (BLI). Mice were randomized and received either vehicle (n = 8) or anti-sclerostin antibody (Scl-Ab; n = 8) once a week for 4 weeks. (**A** and **B**) Tumor growth in bone was visualized after 4 weeks of treatment (**A**) and quantified (**B**) by BLI. Values are represented in a $\log_{10}$ scale. (**C** and **D**) Quantification of the metastasis area (**C**) in the tibia (**D**) of cancer-bearing mice treated with vehicle (n = 16 tibiae) or Scl-Ab (n = 16 tibiae) using histological sections. Scale bar: 1 mm. (**E** and **F**) Quantification of human leukocyte antigen (*HLA*) mRNA expression in the lung (**E**) and brain (**F**) by qRT-PCR (n = 8). (**G**) Kaplan-Meier survival curve of cancer-bearing mice treated with vehicle (n = 6) or Scl-Ab (n = 6). Data are presented as mean ± SEM. Two groups were compared using 2-tailed Student's t test; $^*P < 0.05$.

was greatly reduced by Scl-Ab treatment (Figure 5A), suggesting that the presence of breast cancer bone metastases activates the p38/NF-κB signaling cascade, which is attenuated by inhibition of sclerostin.

To determine whether sclerostin directly activates the p38/NF-κB signaling pathway in myoblasts, we stimulated C2C12 myoblasts with recombinant sclerostin. Sclerostin treatment did not induce phosphorylation of p38 or the components of the NF-κB pathway (Supplemental Figure 5B and data not shown), suggesting that the pathway is activated indirectly by cytokines present in the metastatic microenvironment.

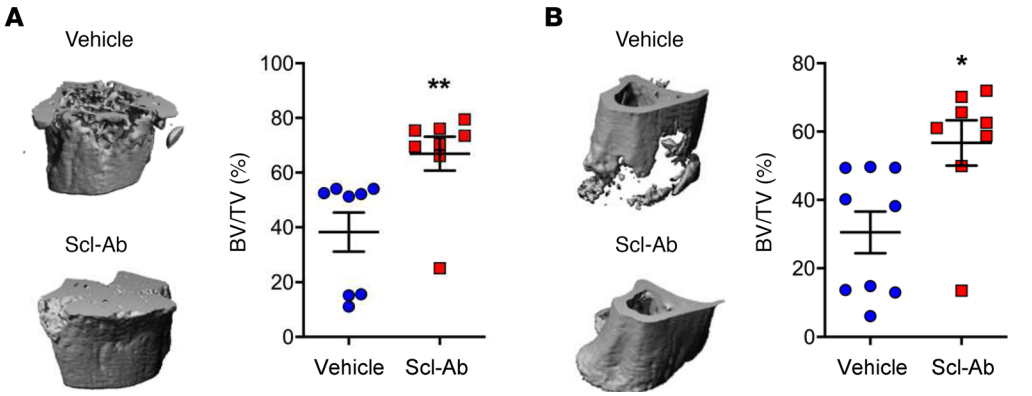
A
Vehicle
Scl-Ab
BV/TV (%)
Vehicle
Scl-Ab
B
Vehicle
Scl-Ab
BV/TV (%)
Vehicle
Scl-Ab

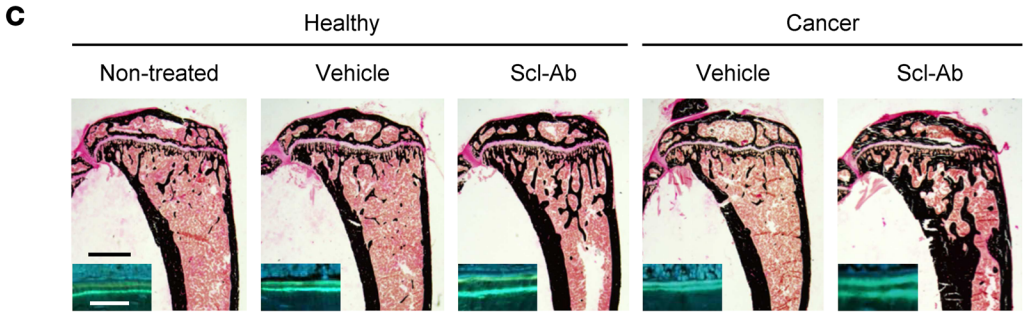
C
Healthy
Cancer
Non-treated
Vehicle
Scl-Ab
Vehicle
Scl-Ab

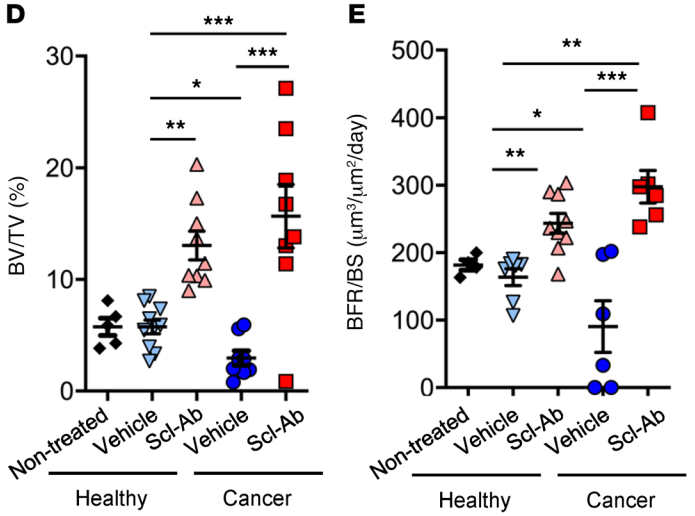
D
BV/TV (%)
Non-treated
Vehicle
Scl-Ab
Vehicle
Scl-Ab
Healthy
Cancer
E
BFR/BS (μm³/μm²/day)
Non-treated
Vehicle
Scl-Ab
Vehicle
Scl-Ab
Healthy
Cancer

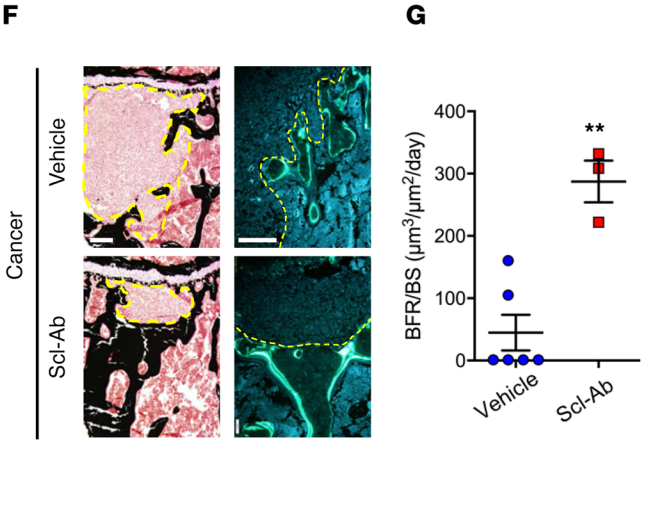
F
Cancer
Vehicle
Scl-Ab
G
BFR/BS (μm³/μm²/day)
Vehicle
Scl-Ab

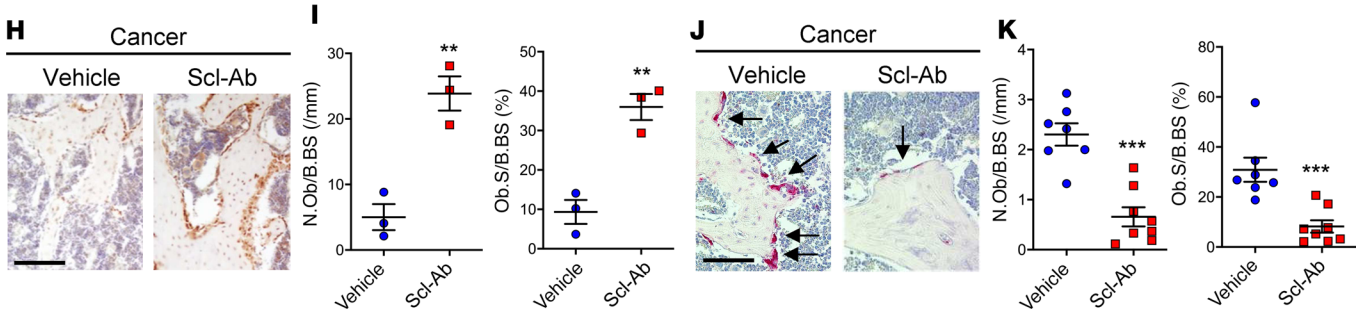
H
Cancer
Vehicle
Scl-Ab
I
N.Ob/B.BS (/mm)
Ob.S/B.BS (%)
Vehicle
Scl-Ab
J
Cancer
Vehicle
Scl-Ab
K
N.Ob/B.BS (/mm)
Ob.S/B.BS (%)
Vehicle
Scl-Ab

Figure 3. Anti-sclerostin antibody treatment protects from breast cancer–induced bone destruction. (**A** and **B**) Microcomputed tomography (μCT) analysis of bone mass (BV/TV, bone volume/total volume) of the femur (**A**) and tibia (**B**) of cancer-bearing mice treated with vehicle (n = 8) or anti-sclerostin antibody (Scl-Ab; n = 8). (**C**) Von Kossa/van Gieson staining of proximal tibiae and fluorescence double labeling (insets) from healthy mice and cancer-bearing mice treated with vehicle or Scl-Ab. Scale bars: 1 mm (black) and 50 μm (white). (**D**) Histomorphometric analysis of bone mass (BV/TV, bone volume/tissue volume) of the proximal tibia (healthy nontreated n = 5, vehicle-treated n = 10, Scl-Ab–treated n = 10; cancer-bearing vehicle-treated n = 8, cancer-bearing Scl-Ab–treated n = 8). (**E**) Analysis of bone formation rate (BFR/BS, bone formation rate/bone surface) of the proximal tibia. (**F**) Von Kossa/van Gieson staining (2 left panels) of the proximal tibia of mice with bone metastases and calcein double labeling (2 right panels) at the bone-cancer interface. Scale bars: 50 μm. (**G**) BFR/BS at the bone-cancer interface (vehicle n = 6, Scl-Ab n = 3). (**H**) Immunohistochemical staining of osterix in the distal femur of cancer-bearing mice treated with vehicle or Scl-Ab. Scale bar: 50 μm. (**I**) Histomorphometric analysis of the distal femur (N.Ob/BS, number of osteoblasts per bone surface; Ob.S/BS, osteoblast surface per bone surface) (vehicle n = 6, Scl-Ab n = 3). (**J**) Tartrate-resistant acid phosphatase (TRAP) staining of the distal femur of cancer-bearing mice treated with vehicle or Scl-Ab. Scale bar: 50 μm. (**K**) Quantification of osteoclasts per bone surface (N.Oc/BS) and of the osteoclast surface per bone surface (Oc.S/BS) (vehicle n = 8, Scl-Ab n = 8). Data are presented as mean ± SEM. Two-tailed Student's t test was used to compare 2 groups (**A**, **B**, **G**, **I**, and **K**), and ANOVA followed by Tukey's post hoc analysis was used to compare 3 or more groups (**D** and **E**); $^{*}P < 0.05$, $^{**}P < 0.01$, $^{***}P < 0.001$.

TGF-β1 is an abundant growth factor released from the bone matrix during breast cancer–induced bone resorption. Interestingly, stimulation of undifferentiated C2C12 myoblasts with TGF-β1 activated the p38/NF-κB pathway, thus recapitulating the effect observed in muscles of cancer-bearing mice (Figure 5B). Inhibition of the NF-κB pathway abrogated TGF-β1–induced phosphorylation of p38 (Figure 5C), suggesting that the effect of TGF-β1 was at least in part mediated via NF-κB. Consistently, TGF-β1 stimulation inhibited the differentiation of C2C12 myoblasts into myocytes, as determined by reduced expression of *myogenin* and *MyoD* (Figure 5D). These data suggest that TGF-β1 released from the bone matrix during osteolytic bone resorption reduces muscle function, which is prevented by Scl-Ab treatment. Indeed, expression of the TGF-β1 target gene Pai1 was significantly increased in muscles of bone metastasis–bearing mice compared with healthy animals (Figure 5E). However, Pai1 expression was not increased in the muscles of Scl-Ab–treated tumor-bearing mice (Figure 5E), indicating that Scl-Ab treatment restores the breast cancer-induced activation of the TGF-β1 and p38/NF-κB pathway.

In colon cancer, NF-κB accumulation prevents the downregulation of Pax7, leading to a compromised muscle regeneration and impaired skeletal muscle function (29). To address the question of whether this also occurs in mice with breast cancer bone metastases, we analyzed the number of Pax7-positive satellite cells in the TA muscles. Interestingly, the number of Pax7-positive cells was significantly increased in cancer-bearing mice compared with healthy animals (Figure 5, F and G). This cancer-induced increase was partially but significantly reversed by Scl-Ab treatment (Figure 5G). Together, these data suggest that pharmacological inhibition of sclerostin protects from breast cancer–induced loss of muscle function by preventing the cancer-mediated activation of NF-κB signaling and the subsequent increase in Pax7-positive satellite cells.

Discussion

In the present study, we report that MDA-MB-231 metastatic breast cancer cells secrete sclerostin, a soluble glycoprotein that binds to Lrp5/6 on osteoblasts and prevents the activation of the Lrp5/6-frizzled receptor complex by soluble Wnt ligands and subsequent activation of the canonical Wnt signaling pathway (11). In vitro assays revealed that metastatic breast cancer cell–derived sclerostin restricts osteoblast differentiation. In vivo inhibition of sclerostin using a monoclonal anti-sclerostin antibody (Scl-Ab) reduced bone metastatic burden and protected from breast cancer–induced bone destruction. At the tissue level, inhibition of sclerostin increased bone formation rate and bone mass in both healthy and cancer-bearing mice. In mice with bone metastases, sclerostin inhibition increased osteoblast number and bone formation rate, while the number and activity of osteoclasts were decreased. Together these effects restricted tumor burden and osteolytic bone destruction, thereby increasing the survival time of cancer-bearing mice.

Muscle weakness is known to accompany metastatic breast cancer disease (17, 30), which was confirmed in our model system. Interestingly, while Scl-Ab treatment did not affect the function of healthy muscle, the decreased strength and endurance of muscles obtained from mice with breast cancer bone metastases were reconstituted to the performance of muscles obtained from healthy mice. At the tissue level, sclerostin inhibition restored the relative smaller size of oxidative and nonoxidative muscle fibers in cancer-bearing mice. Molecularly, similar to the results found by stimulation with TGF-β1, metastatic bone disease activated p38/NF-κB signaling and increased the number of Pax7-positive satellite cells in muscle tissue, which was largely abrogated by Scl-Ab treatment.

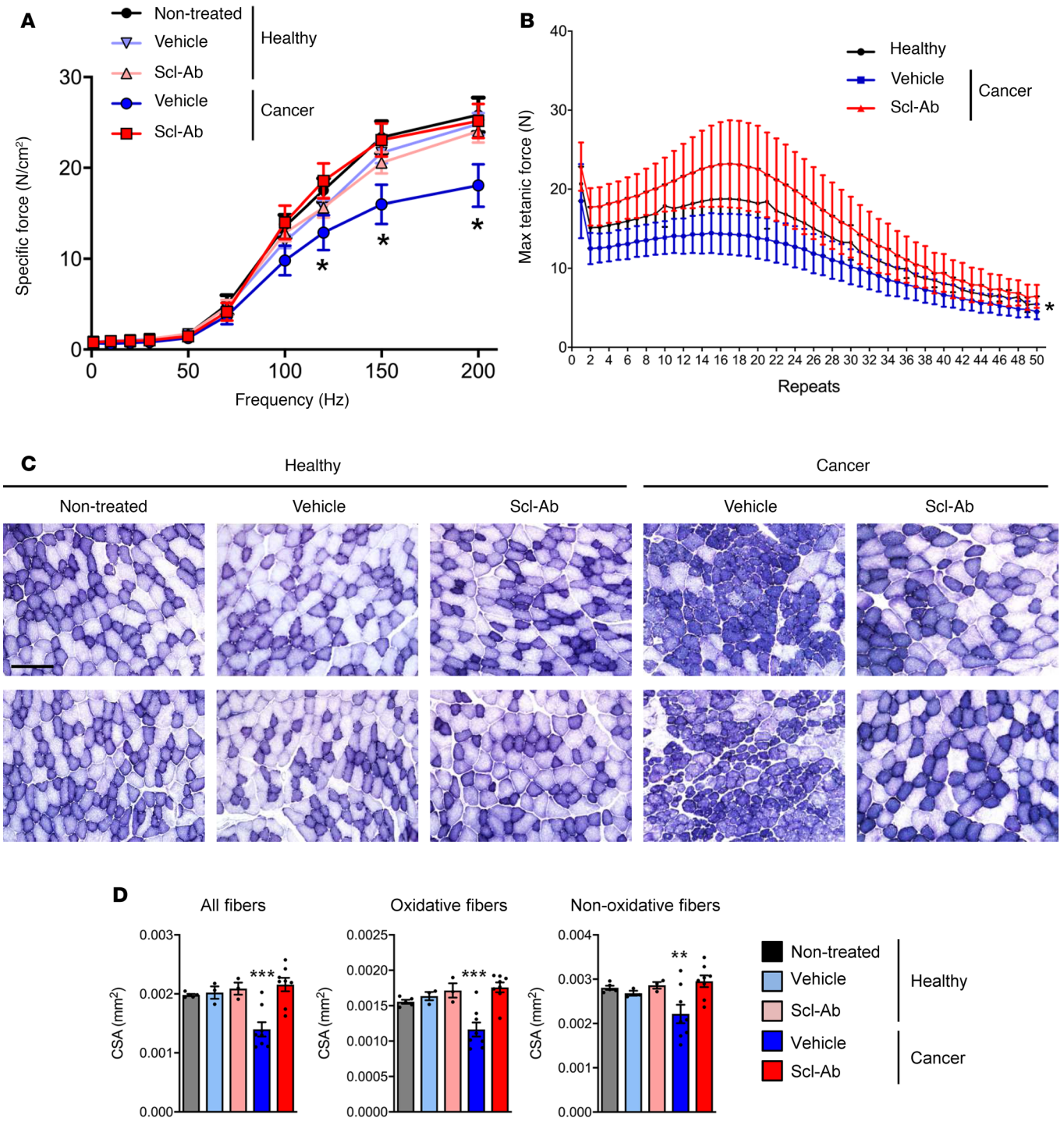

Figure 4. Inhibition of sclerostin prevents breast cancer–induced loss of muscle function. (**A**) Specific force of the extensor digitorum longus (EDL) muscle from healthy mice without treatment (n = 5), or treated with vehicle (n = 10) or anti-sclerostin antibody (Scl-Ab, n = 10); and from cancer-bearing mice treated with vehicle (n = 8) or Scl-Ab (n = 8). N, newtons. (**B**) Endurance of the EDL muscle of mice with bone metastases treated with vehicle (n = 8) or Scl-Ab (n = 8). max, maximum. (**C**) Succinate dehydroxygenase–stained (SDH-stained) tibialis anterior muscle sections from healthy mice without treatment or with vehicle or Scl-Ab treatment, as well as from mice with bone metastases treated with vehicle or Scl-Ab stained. Two representative muscles are shown per group. Scale bar: 50 μm. (**D**) Quantification of the cross-sectional area (CSA) of all muscle fibers, oxidative fibers, and nonoxidative fibers using SDH-stained muscle sections from healthy mice without treatment (n = 5), or with vehicle (n = 10) or Scl-Ab treatment (n = 10); and from cancer-bearing mice treated with vehicle (n = 8) or Scl-Ab (n = 8). Data are presented as mean ± SEM. Three or more groups were compared using ANOVA followed by Tukey's post hoc analysis; $^{*}P < 0.05$, $^{**}P < 0.01$, $^{***}P < 0.001$.

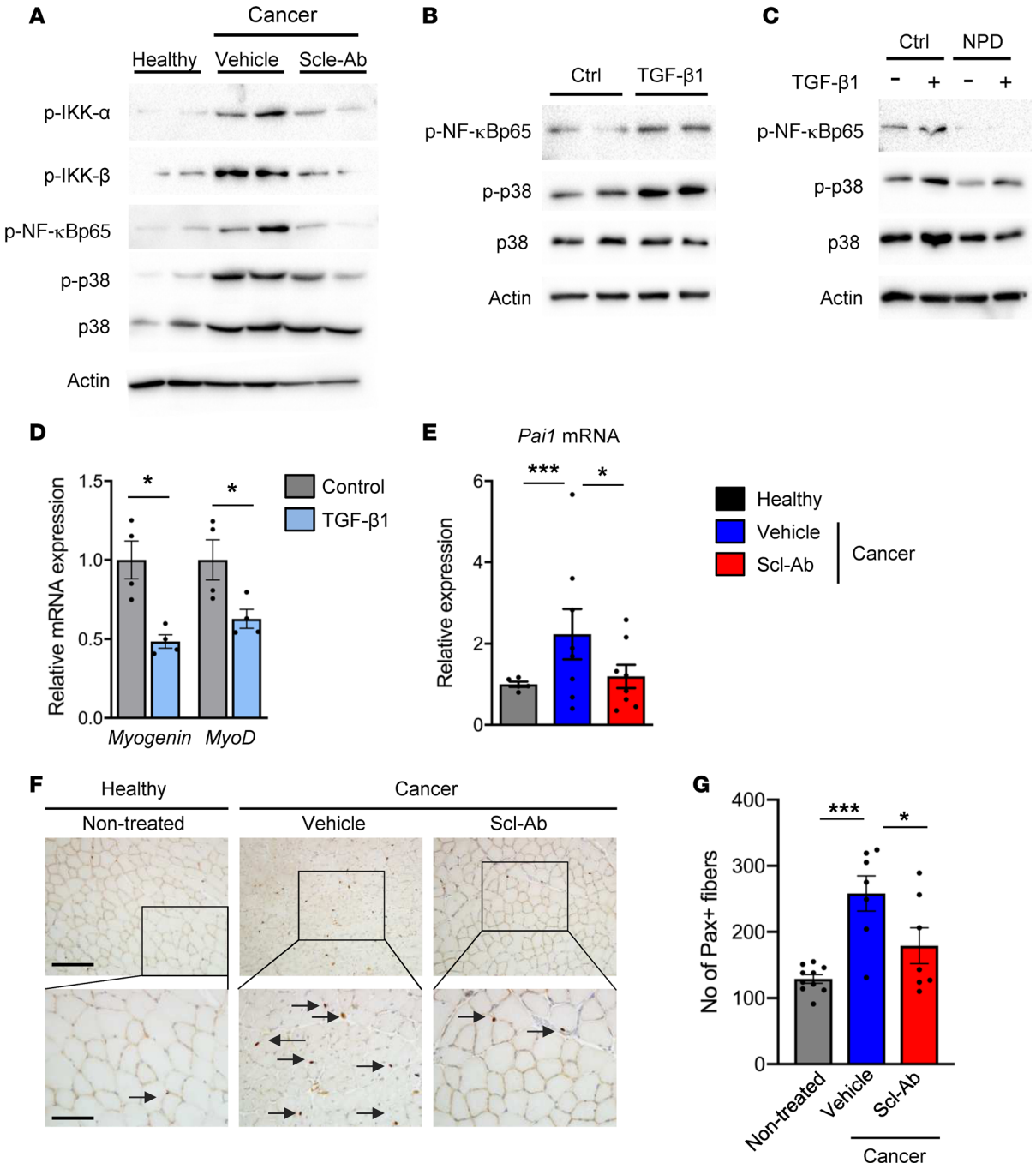

Figure 5. Treatment with an anti-sclerostin antibody reverses breast cancer–induced activation of NF-κB signaling and increased number of Pax7-positive cells. (**A**) Immunoblot analysis of phosphorylated IKKα and IKKβ (p-IKKα and p-IKKβ), phosphorylated NF-κBp65 (p-NF-κBp65), phosphorylated p38 (p-p38), and total p38 in the gastrocnemius (GAS) muscle of healthy nontreated mice (n = 5) and cancer-bearing mice treated with vehicle (n = 8) or Scl-Ab (n = 8). Actin was used as loading control. Representative samples are shown. (**B**) Immunoblot analysis of phosphorylated NF-κBp65 (p-NF-κBp65), phosphorylated p38 (p-p38) and total p38 in C2C12 myoblasts stimulated with vehicle (veh) or TGF-β1. Actin was used as loading control. Representative image of 6 independent experiments is shown. (**C**) Immunoblot analysis of phosphorylated NF-κBp65, p-p38, and total p38 in C2C12 cells treated with a control peptide or an NF-κB blocking peptide (NPD) and stimulated with vehicle or TGF-β1. Actin was used as loading control. Representative image of 4 independent experiments is shown. (**D**) *Myogenin* and *MyoD* mRNA expression was quantified by qRT-PCR in C2C12 cells after 10 days of myogenic differentiation (n = 4). (**E**) *Pai1* mRNA expression was quantified in the GAS muscle from healthy nontreated mice (n = 5) and from cancer-bearing mice treated with vehicle (n = 8) or Scl-Ab (n = 8). (**F**) Immunohistochemical staining of Pax7 in the tibialis anterior (TA) muscle from healthy nontreated mice and from mice with bone metastases treated with vehicle or Scl-Ab. Scale bar: 50 μm (top row) and 100 μm (bottom row). (**G**) Quantification of Pax7-positive cells in the TA muscle from healthy nontreated mice (n = 5) and from mice with bone metastases treated with vehicle (n = 8) or Scl-Ab (n = 8). Data are presented as mean ± SEM. Two-tailed Student's t test was used to compare 2 groups (**D**), and ANOVA followed by Tukey's post hoc analysis was used to compare 3 or more groups (**E** and **G**); $^*P < 0.05$, $^{***}P < 0.001$.

Breast cancer is a devastating disease of high prevalence, with a great potential to metastasize to bone. Bone metastases cause osteolytic lesions that lead to pain, pathologic fractures, and muscle weakness (17, 18). These conditions are accompanied by high morbidity and mortality and an overall reduced survival rate (8). Current treatments are effective in reducing the progression of osteolytic lesions but do not reverse bone destruction or improve muscle weakness, demonstrating the need for additional therapeutic options. In breast cancer–induced bone disease, it is firmly established that breast cancer cells create a hostile microenvironment by secreting soluble factors that increase the number and activity of bone-resorbing osteoclasts that eventually cause bone destruction (5). While some secreted factors including interleukins directly activate osteoclasts, other factors such as PTHrP stimulate osteoblasts to secrete RANKL, which in turn augments osteoclast activity and bone resorption (5). The activated bone resorption releases matrix-derived growth factors such as TGF-β1 that enhance cancer cell proliferation and further activate osteoclast activity and bone resorption, thereby establishing a feed-forward loop (5). In this context, osteoblasts mainly assume a passive role as recipients and sources of growth factors. However, recent evidence and data reported in this study also suggest an active role of osteoblasts during the establishment and expansion of multiple myeloma and breast cancer (27, 31). For instance, myeloma cells have been reported to inhibit bone formation, which is relieved by Scl-Ab treatment (27, 31). In contrast to breast cancer cells, myeloma cells do not express sclerostin, and the inhibition of bone formation is likely mediated by Dkk1 and other factors (27, 31). Thus, augmentation of bone formation by Scl-Ab treatment is likely caused by antagonizing osteocyte-derived sclerostin.

In metastatic breast cancer, it was shown that sclerostin is derived from metastatic tissue in addition to osteocytes (32). This is consistent with our findings showing that metastatic MDA-MB-231 breast cancer cells and several other triple-negative breast cancer cells express sclerostin, while nonmetastatic or hormone receptor–positive breast cancer cells do not express sclerostin. ER signaling has been shown to reduce sclerostin expression (33). Whether low sclerostin expression in ER-positive breast cancer cells is due to estrogen signaling remains to be elucidated. However, it is possible that the lack of the ER is permissive for sclerostin expression in aggressive triple-negative cells. In the present study, sclerostin expression was analyzed in a restricted number of primary breast cancer tissue biopsies. Thus, investigating the expression of sclerostin in a larger patient cohort and in bone metastases would be useful to determine whether sclerostin expression correlates with the hormone receptor status and bone metastatic burden. Nevertheless, our results suggest that sclerostin expression might be an important functional feature of malignancy in triple-negative breast cancer that is likely to contribute to the deregulation of the local metastatic microenvironment and potentially to distant effects of bone metastases. Triple-negative breast cancer represents approximately 10%–15% of all breast cancers, and patients have high risk of relapse and poor survival compared with those with breast cancers expressing hormone receptors or HER-2/neu (34). The good prognosis of hormone receptor–positive and HER-2/neu–amplified tumors is largely due to advances made in targeted therapies, i.e., agents that interfere with hormone production/action or inhibit HER-2/neu, respectively (35). Unfortunately, there are no targeted therapies recommended for triple-negative breast cancer, and the prevailing treatment remains to be standard chemotherapy. Thus, identification of sclerostin expression in a subset of triple-negative breast cancers might be of translational relevance for the development of improved treatment options.

Our experiments reveal that MDA-MB-231 metastatic breast cancer cell–derived sclerostin binds to Lrp5 on osteoblasts, leading to inhibition of canonical Wnt signaling and osteoblast differentiation. By this mechanism, metastatic breast cancer cells are likely to suppress osteoblast activity and bone formation in vivo, a component that might contribute to metastatic bone destruction by favoring osteoclast-dependent bone resorption over osteoblast-mediated bone formation. In addition to augmenting osteoblast function and bone formation, sclerostin inhibition using Scl-Ab strongly reduced the osteoclast number and activity. These findings are consistent with phase II and III clinical trials in which postmenopausal women with osteoporosis were treated with an anti-sclerostin antibody to increase BMD (36, 37). The decline in bone resorption might be due to increased expression of the Wnt target gene osteoprotegerin (OPG), which acts as a decoy receptor to RANKL and decreases the RANKL/OPG ratio and bone resorption (38). The dual osteoanabolic and antiresorptive effect most likely contributes to the increase in bone mass and to the attenuation of bone destruction in the context of the osteolytic disease. Indeed, Scl-Ab treatment of mice bearing bone metastases greatly reduced the metastatic burden compared with vehicle-treated mice. Reduction of bone metastases did not increase metastasis formation at other sites, leading to a decrease in overall metastatic burden. Importantly, Scl-Ab treatment of metastasis-bearing mice prolonged overall survival.

Patients with advanced metastatic breast cancer often experience a wasting condition in which skeletal muscle undergoes atrophy, leading to pronounced weight loss and ultimately cachexia (39, 40). In the muscle microenvironment, Pax7-positive satellite cells are the main resident stem cells that can give rise to myocytes (41). In addition, other interstitial and perivascular cell populations can also enter the myogenic lineage and contribute to muscle repair in response to tissue damage (42). Muscle damage can be a consequence of cachexia that is associated with an expansion and activation of Pax7-positive interstitial satellite cells and type 2 fiber atrophy (43). Satellite cell activation is indicated by an increased abundance of desmin and phospho-p38α (44). Under normal conditions, satellite cells are positioned between the myofiber sarcolemma and the basal lamina, but exit from quiescence upon muscle damage along with other myogenic progenitor populations and subsequently expand as myoblasts to repair damaged fibers (45). Perturbation of the sarcolemma and the basal lamina as well as satellite cell activation in cachectic muscle is not due to the spreading of tumor cells but rather caused by circulating factors including TGF-β1 (17). Serum-derived cachectic factors activate NF-κB signaling in myogenic progenitors upstream of Pax7, which becomes upregulated and suppresses expression of MyoD and myogenin. This mechanism blocks myogenic differentiation and myoblast fusion and promotes muscle wasting (29). Furthermore, it has been demonstrated that the increase in circulating TGF-β1 in the context of osteolytic disease upregulated NADPH oxidase 4 in skeletal muscle, causing an oxidation of the ryanodine receptor and calcium (Ca^{2+}) release channel (RyR1) (17). Oxidation of RyR1 leads to Ca^{2+} leakage and an impairment of muscle contraction (17). These findings strongly indicate that several molecular mechanisms exist that contribute to a cancer- and bone metastasis–mediated decline in muscle function and ultimately cachexia.

In the present study, we report that mice with breast cancer bone metastases have reduced muscle strength and endurance and demonstrate that the muscle weakness is fully abrogated by treatment with Scl-Ab. Our data are consistent with findings reported by others and demonstrate that advanced stages of malignancy and bone metastases cause muscle weakness (17). However, the use of Scl-Ab to improve muscle function has not to our knowledge been reported thus far but would be of great clinical interest. At the tissue level, advanced malignancy with bone metastases caused a reduction in the size of oxidative and nonoxidative muscle fibers. Antagonizing sclerostin activity reversed muscle fiber atrophy, thereby normalizing the tissue microarchitecture. Molecularly, cancer-induced muscle fiber atrophy was associated with increased NF-κB and p38 signaling that was also induced by TGF-β1 and normalized by Scl-Ab treatment. Stimulation with TGF-β1 also reduced myogenin expression and myoblast differentiation. These findings suggest that enhanced osteoclast activity in the bone cancer microenvironment increases the serum concentration of bone matrix–derived TGF-β1, and impairs myogenin expression and muscle regeneration downstream of NF-κB and p38 signaling. Indeed, TGF-β1 pathway activity was increased in muscle tissue as evidenced by increased Pai-1 expression, which was at least in part reconstituted by sclerostin inhibition. Furthermore, the number of Pax7-positive satellite cells was strikingly increased in tumor-bearing mice and almost normalized by Scl-Ab treatment. We therefore propose that the bone-forming effect and antiresorptive properties of anti-sclerostin treatment both contribute to a reduction in osteolytic bone destruction and extension of survival time, while the anticatabolic effect mainly contributes to restoration of muscle function by preventing an increase in TGF-β1 concentration.

Consistent with other reports, we demonstrated that Scl-Ab treatment has a bone-sparing effect and reduces bone destruction in the context of a malignant bone disease that disturbs the balance of the bone microenvironment. Muscle fiber atrophy and muscle weakness, which often accompany metastatic breast cancer, were also prevented by pharmacological inhibition of sclerostin. These features are clinically relevant and may improve the current treatment options for patients with breast cancer bone metastases. In all preclinical and clinical studies that are available thus far, Scl-Ab treatment has been proven safe with regard to malignant side effects. Its clinical use might therefore be possible even with a history of a malignant disease or an actual cancer diagnosis, which is a great advantage over the currently available bone-anabolic drugs PTH 1-34 (teriparatide; Forteo/Forsteo, Eli Lilly and Co.) and PTHrP (abaloparatide; Tymlos, Radius) (6). It would therefore be of great interest to investigate, in a clinical context, whether sclerostin inhibition is also beneficial for patients with breast cancer bone metastases. This would expand the repertoire of oncological treatment options for and improve the bone health of breast cancer patients.

Methods

Animal experiments. MDA-MB-231 breast cancer cells stably expressing the luciferase have been described elsewhere (46) and were injected into the left ventricle of 8-week-old female immune-compromised CB-17/lcr-Prkdc^{scid}/Rj mice (Janvier Laboratories). Bioluminescence imaging (BLI) was performed 2 weeks after breast cancer cell injection using an IVIS 200 imaging system (PerkinElmer), and mice were randomized into 2 treatment arms. One group (n = 8) received vehicle (50 µl/10 g mouse), and the other group (n = 8) Scl-Ab (100 mg/kg; BPS-804, setrusumab; Mereo BioPharma) i.v. once a week for 4 weeks. Tumor burden was measured weekly by BLI. Mice were sacrificed 1 week after the last injection. In the survival study, mice were treated once a week with vehicle (n = 6) or Scl-Ab (n = 6), monitored daily, and sacrificed once well-defined criteria such as 20% weight loss were reached. Healthy CB-17/lcr-Prkdc^{scid}/Rj mice without treatment (n = 10), or treated with vehicle (n = 10) or Scl-Ab (n = 10) served as controls. Investigators were blinded to the group allocation.

µCT. µCT was used for 3D analyses of long bones. Long bones of mice were analyzed using high-resolution µCT with a fixed isotropic voxel size of 10 µm (70 peak kV at X µA 400 ms integration time; Viva80 microCT; Scanco Medical). All analyses were performed on digitally extracted bone tissue using 3D distance techniques (Scanco Medical) as reported previously (47). Region of interest (ROI) was defined manually by drawing contours in slices. Due to cancer-induced bone destruction and absence of intact bone surfaces in cancer-bearing mice, the ROI contained both cortical and the trabecular bone. In non-cancer-bearing bones, only trabecular bone was analyzed using a standard method (47).

Ex vivo analysis of muscle function. Ex vivo contractility of EDL muscle was analyzed using a device dedicated to the measurement of mouse muscle properties in situ, ex vivo, and in vivo (Aurora Scientific). For this purpose, EDL was dissected from the hind limb, loops were tied to the tendons of the muscles, and mounted to a force transducer. Muscles were stimulated to contract using a supramaximal stimulus applied by 2 electrodes. For fatigue studies, EDL was stimulated with 70 Hz for 50 repeats, and the maximum tetanic force was detected. Data were collected and analyzed using Dynamic Muscle Control/Data Acquisition (DMC) and Dynamic Muscle Control Data Analysis (DMA) programs (Aurora Scientific). Specific muscle force was calculated as described previously (48). Investigators were blinded regarding the treatment during data analysis.

Histological and immunohistochemical analyses. For bone analyses, mice were injected 7 and 2 days prior to sacrifice with calcein (20 mg/kg) and demeclocycline (20 mg/kg; both Sigma-Aldrich), respectively. Tibiae were collected and fixed in 4% paraformaldehyde (PFA) for 48 hours. For histomorphometric analysis, tibiae were embedded in methyl methacrylate. Toluidine blue, von Kossa/van Gieson and TRAP staining were performed using 5-µm sagittal sections. Quantitative bone histomorphometric measurements were performed according to standard protocols using an OsteoMeasure system (Osteometrics) (49). Femurs were cleaned from soft tissue, fixed in 4% PFA for 24 hours at 4°C, decalcified with 4% EDTA for 4 days and 20% EDTA for 24 hours, and embedded in paraffin. Sections were cut, and immunohistochemical staining was performed using an anti-Osterix antibody (rabbit polyclonal; Santa Cruz Biotechnology). Brain and lung tissues were fixed in 4% PFA for 24 hours at 4°C. Tissue samples were embedded in paraffin and cut, and immunohistochemical staining was performed with an antibody against HLA class 1 ABC (mouse monoclonal, Abcam).

For histological analyses of muscle tissues, the TA muscle was dissected from the hind limb, embedded in 10% Gum Tragacanth, and snap-frozen in cooled 2-methylbutane. Cryosections were prepared using a cryotome, and sections were stained for succinate dehydroxygenase (SDH). Pax7 staining was performed using an anti-Pax7 antibody (mouse monoclonal; Developmental Studies Hybridoma Bank [DSHB]). Muscle fiber area and number of Pax7-positive cells were quantified using the Osteomeasure system (Osteometrics). The investigators were blinded regarding the treatment.

Cell culture. For calvarial osteoblast cultures, calvariae were dissected from 1- to 3-day-old mice and digested sequentially in α-MEM containing 0.1% collagenase and 0.2% dispase (both Roche). Cell fractions 2–4 were combined and expanded in α-MEM (Invitrogen) containing 10% FBS (Invitrogen) and 100 U/ml penicillin, 100 µg/ml streptomycin (Invitrogen). C2C12 cells were purchased from DSMZ and cultured in DMEM (Invitrogen) containing 10% FBS and 1% penicillin/streptomycin. Cells were stimulated with 10 ng/ml TGF-β1 (R&D Systems) or 100 ng/ml recombinant sclerostin (R&D Systems). To inhibit NF-κB signaling in C2C12 cells, cells were pretreated for 1 hour with NEMO-binding domain peptide (NPD, Enzo) or L-TAT control peptide (Enzo). Myocyte differentiation was induced using DMEM supplemented with 2% horse serum (Invitrogen) and 1% penicillin/streptomycin. MCF-7 and MDA-MB-231 breast cancer cells were purchased from ATCC. MCF-7 cells were cultured in DMEM (Invitrogen), and

Table 2. Antibodies used in this study

Antibody	Host animal	Dilution	Source	Catalog no.	Application
Pax7	Mouse	1:10	DSHB	–	IHC
HLA	Mouse	1:100	Abcam	ab70328	IHC
Osterix	Rabbit	1:500	Santa Cruz Biotechnology	Sc-22536-R	IHC
p38	Rabbit	1:500	Cell Signaling Technology	8690	IB
Phospho-p38	Rabbit	1:500	Cell Signaling Technology	4511	IB
Phospho-IKKα	Rabbit	1:500	Elabscience	E-AB-20902	IB
Phospho-IKKβ	Rabbit	1:500	Elabscience	E-AB-20903	IB
Phospho–NF-κB p65	Rabbit	1:500	Abcam	ab28856	IB
Actin	Mouse	1:5000	Millipore	MAB1501	IB
p44/42 MAPK (Erk1/2)	Mouse	1:1000	Cell Signaling Technology	9107	IB
Phospho–p44/42 MAPK (Erk1/2) (Thr202/204)	Rabbit	1:1000	Cell Signaling Technology	4370	IB
STAT3	Mouse	1:500	Cell Signaling Technology	9139	IB
Phospho–STAT3 (Tyr705)	Rabbit	1:500	Cell Signaling Technology	9145	IB

MDA-MB-231 cells were grown in α-MEM, both supplemented with 10% FBS and 1% penicillin/streptomycin. All cell lines were tested for mycoplasma contamination. MDA-MB-231 cells were transfected with scrambled control siRNA or siRNA against sclerostin (Origene) using Lipofectamine 3000 (Thermo Fisher Scientific) according to the manufacturer's instructions. For collection of conditioned medium, MDA-MB-231 cells were cultured in the presence of 1% FBS for 24 hours, and conditioned medium was collected and stored at –80°C. Osteoblast differentiation was induced by supplementing α-MEM with 0.2 mM L-ascorbic acid and 10 mM β-glycerophosphate (both Millipore). Osteoblast differentiation was determined by staining the cells with 40 mM alizarin red S (AR-S; Sigma-Aldrich) solution at pH 4.2 for 10 minutes at room temperature after fixing the cells in 4% neutrally buffered formaldehyde solution. To determine Wnt signaling activity, calvarial osteoblasts were transfected with TOPflash and *Renilla* plasmids using the Neon System (Invitrogen). Luciferase activity was measured using the Promega Dual Luciferase kit following the manufacturer's guidelines.

RNA isolation and qRT-PCR. Lung and brain tissues were snap-frozen in liquid nitrogen, and RNA was isolated using Trizol. RNA was isolated from cultured cells using the RNeasy Plus Mini Kit (QIAGEN). cDNA was synthesized using the NEB ProtoScript II First Strand cDNA Synthesis kit according to the manufacturer's instructions. Expression of *myogenin, MyoD*, *Pai1*, *SOST*, and the human leukocyte antigen (*HLA*) gene was quantified by qRT-PCR. After normalization to *GAPDH* mRNA, the relative expression level of each target gene was calculated using the comparative CT method.

Expression analysis in human tissue. *SOST* expression in 48 human breast cancer tissues was analyzed using the TissueScan Breast Cancer Array III (Origene) according to the manufacturer's instructions. TissueScan Cancer Survey Array 96 I (Origene), consisting of 72 tumor samples and 24 nonmalignant tissue samples from 8 different primary organs, was utilized to analyze the expression pattern of *SOST* in various malignant tissues. Expression of *SOST* was quantified using qRT-PCR. *Beta-actin* (*ACTB*) was used as an internal control.

Immunoblotting. Cells were lysed in low-salt lysis buffer (pH 7.6) containing 50 mM Tris base, 150 mM NaCl, 0,5% Nonindet P-40 (NP-40), 0.25% sodium deoxycholate, and complete protease and phosphatase inhibitors (Roche). Muscle tissue was homogenized in lysis buffer (20 mM Tris, pH 7.8, 137 mM NaCl, 2.7 mM KCl, 1 mM $MgCl_2$, 1% Triton X-100, 10% glycerol, 1 mM EDTA, 1 mM dithiothreitol, and protease and phosphatase inhibitors) using a Dounce homogenizer. Lysates were separated on 12% polyacrylamide gels and subjected to immunoblot analysis. Immunoblots were incubated overnight at 4°C with primary antibodies listed in Table 2. Peroxidase-labeled anti-rabbit or anti-mouse secondary antibodies (1:10,000, Santa Cruz Biotechnology, catalog

W401B, W402B) were used to visualize bands using Clarity Western ECL Substrate (Bio-Rad). Images of the immunoblots were acquired using the ChemiDoc imaging system and Image Lab software (Bio-Rad).

ELISA. ELISA was used to determine P1NP and TRAP concentration in mouse serum. All procedures were performed according to the manufacturer's (immunodiagnostics systems) instructions.

Statistics. Parametric data were analyzed using 2-tailed Student's *t* test when 2 groups were compared. ANOVA was used when more than 2 groups were compared, followed by Tukey's post hoc analysis to compare the groups. Probability values were considered statistically significant at $P < 0.05$. Experiments were repeated at least 3 times as biological replicates, with a minimum of 2 technical replicates. All quantitative data are presented as mean ± SEM.

Study approval. All animal experiments were conducted in compliance with ethical regulations and according to protocols approved by the local authority for animal welfare (Behörde für Gesundheit und Verbraucherschutz [BVG], Hamburg, Germany).

Author contributions

EH designed research studies, analyzed data, and wrote the manuscript. SS conducted experiments and acquired and analyzed data. DB conducted experiments and acquired and analyzed data. JP conducted experiments and acquired and analyzed data. HS conducted experiments and analyzed data. HT conceived the study, designed research studies, conducted experiments, acquired and analyzed data, and wrote the manuscript.

Acknowledgments

We are indebted to Gudrun Arndt and Philipp Missberger for mouse husbandry and the University Medical Center Hamburg-Eppendorf. We thank Antonio Virgilio Failla of the University Microscopy Imaging Facility (Umif) and Michael Horn-Glander of the University Cancer Center Hamburg (UCCH) Core Facility In Vivo Optical Imaging (CF IVOI) for technical support. We are grateful to Michaela Kneissel and Ina Kramer (Novartis) for providing the Scl-Ab and to Anthony Hall (Mereo BioPharma) for continued permission to use the antibody. EH acknowledges funding from the Deutsche Forschungsgemeinschaft (HE 5208/2-1, HE 5208/2-3). HT obtained funding from the Deutsche Forschungsgemeinschaft (TA 1154/1-1).

Address correspondence to: Hanna Taipaleenmäki, Molecular Skeletal Biology Laboratory, Department of Trauma, Hand and Reconstructive Surgery, University Medical Center Hamburg-Eppendorf, N27 Research Campus, Martinistrasse 52, D-20246 Hamburg, Germany. Phone: 49.40.7410.51961; Email: h.taipaleenmaeki@uke.de.

1. Pantel K, Brakenhoff RH. Dissecting the metastatic cascade. *Nat Rev Cancer*. 2004;4(6):448–456.
2. Roodman GD. Mechanisms of bone metastasis. *N Engl J Med*. 2004;350(16):1655–1664.
3. Coleman RE, et al. Metastasis and bone loss: advancing treatment and prevention. *Cancer Treat Rev*. 2010;36(8):615–620.
4. Clines GA, Guise TA. Molecular mechanisms and treatment of bone metastasis. *Expert Rev Mol Med*. 2008;10:e7.
5. Weilbaecher KN, Guise TA, McCauley LK. Cancer to bone: a fatal attraction. *Nat Rev*. 2011;11(6):411–425.
6. Chen Y-C, Sosnoski DM, Mastro AM. Breast cancer metastasis to the bone: mechanisms of bone loss. *Breast Cancer Res*. 2010;12(6):215.
7. Stopeck AT et al. Denosumab compared with zoledronic acid for the treatment of bone metastases in patients with advanced breast cancer: a randomized, double-blind study. *J Clin Oncol*. 2010;28(35):5132–5139.
8. Coleman RE. Impact of bone-targeted treatments on skeletal morbidity and survival in breast cancer. *Oncology (Williston Park)*. 2016;30(8):695–702.
9. Vallet S, Smith MR, Raje N. Novel bone-targeted strategies in oncology. *Clin Cancer Res*. 2010;16(16):4084–4093.
10. Baron R, Hesse E. Update on bone anabolics in osteoporosis treatment: rationale, current status, and perspectives. *J Clin Endocrinol Metab*. 2012;97(2):311–325.
11. Baron R, Kneissel M. WNT signaling in bone homeostasis and disease: from human mutations to treatments. *Nat Med*. 2013;19(2):179–192.
12. Ferrari SL. Osteoporosis: romosozumab to rebuild the foundations of bone strength. *Nat Rev Rheumatol*. 2018;14(3):128–128.
13. McClung MR et al. Romosozumab in postmenopausal women with low bone mineral density. *N Engl J Med*. 2014;370(5):412–420.
14. Sølling ASK, Harsløf T, Langdahl B. The clinical potential of romosozumab for the prevention of fractures in postmenopausal women with osteoporosis. *Ther Adv Musculoskelet Dis*. 2018;10(5–6):105–115.
15. Forlino A, Marini JC. Osteogenesis imperfecta. *Lancet*. 2016;387(10028):1657–1671.
16. Glorieux FH et al. BPS804 anti-sclerostin antibody in adults with moderate osteogenesis imperfecta: results of a randomized phase 2a trial. *J Bone Miner Res*. 2017;32(7):1496–1504.
17. Waning DL et al. Excess TGF-β mediates muscle weakness associated with bone metastases in mice. *Nat Med*.

2015;21(11):1262–1271.
18. Waning DL, Guise TA. Molecular mechanisms of bone metastasis and associated muscle weakness. *Clin Cancer Res*. 2014;20(12):3071–3077.
19. Bu G, et al. Breast cancer-derived Dickkopf1 inhibits osteoblast differentiation and osteoprotegerin expression: implication for breast cancer osteolytic bone metastases. *Int J Cancer*. 2008;123(5):1034–1042.
20. Papatheodorou I et al. Expression Atlas: gene and protein expression across multiple studies and organisms. *Nucleic Acids Res*. 2018;46(D1):D246–D251.
21. Dai X, Cheng H, Bai Z, Li J. Breast cancer cell line classification and its relevance with breast tumor subtyping. *J Cancer*. 2017;8(16):3131–3141.
22. Chavez KJ, Garimella SV, Lipkowitz S. Triple negative breast cancer cell lines: one tool in the search for better treatment of triple negative breast cancer. *Breast Dis*. 2010;32(1-2):35–48.
23. Kurebayashi J et al. Isolation and characterization of a new human breast cancer cell line, KPL-4, expressing the Erb B family receptors and interleukin-6. *Br J Cancer*. 1999;79(5–6):707–717.
24. Semenov MV, He X. LRP5 mutations linked to high bone mass diseases cause reduced LRP5 binding and inhibition by SOST. *J Biol Chem*. 2006;281(50):38276–38284.
25. Boyden LM et al. High bone density due to a mutation in LDL-receptor-related protein 5. *N Engl J Med*. 2002;346(20):1513–1521.
26. Little RD, et al. A mutation in the LDL receptor-related protein 5 gene results in the autosomal dominant high-bone-mass trait. *Am J Hum Genet*. 2002;70(1):11–19.
27. McDonald MM et al. Inhibiting the osteocyte-specific protein sclerostin increases bone mass and fracture resistance in multiple myeloma. *Blood.* 2017;129(26):3452–3464.
28. Jackman RW, Cornwell EW, Wu C-L, Kandarian SC. Nuclear factor-κB signalling and transcriptional regulation in skeletal muscle atrophy. *Exp Physiol*. 2013;98(1):19–24.
29. He WA et al. NF-κB-mediated Pax7 dysregulation in the muscle microenvironment promotes cancer cachexia. *J Clin Invest*. 2013;123(11):4821–4835.
30. Regan JN et al. Osteolytic breast cancer causes skeletal muscle weakness in an immunocompetent syngeneic mouse model. *Front Endocrinol (Lausanne)*. 2017;8:358.
31. Delgado-Calle J et al. Genetic deletion of Sost or pharmacological inhibition of sclerostin prevent multiple myeloma-induced bone disease without affecting tumor growth. *Leukemia*. 2017;31(12):2686–2694.
32. Zhu M et al. Sclerostin induced tumor growth, bone metastasis and osteolysis in breast cancer. *Sci Rep*. 2017;7(1):11399.
33. Galea GL et al. Estrogen receptor α mediates proliferation of osteoblastic cells stimulated by estrogen and mechanical strain, but their acute down-regulation of the wnt antagonist sost is mediated by estrogen receptor β. *J Biol Chem*. 2013;288(13):9035–9048.
34. Wu Q, et al. Breast cancer subtypes predict the preferential site of distant metastases: a SEER based study. *Oncotarget*. 2017;8(17):27990–27996.
35. Gu G, Dustin D, Fuqua SA. Targeted therapy for breast cancer and molecular mechanisms of resistance to treatment. Curr. Opin. *Pharmacol*. 2016;31:97–103.
36. Cosman F et al. Romosozumab treatment in postmenopausal women with osteoporosis. *N Engl J Med*. 2016;375(16):1532–1543.
37. Cosman F, Crittenden DB, Grauer A. Romosozumab treatment in postmenopausal osteoporosis. *N Engl J Med*. 2017;376(4):396–397.
38. Wijenayaka AR et al. Sclerostin stimulates osteocyte support of osteoclast activity by a RANKL-dependent pathway. *PLoS One* 2011;6(10):e25900.
39. Aversa Z, Costelli P, Muscaritoli M. Cancer-induced muscle wasting: latest findings in prevention and treatment. *Ther Adv Med Oncol*. 2017;9(5):369–382.
40. Baracos VE, Martin L, Korc M, Guttridge DC, Fearon KCH. Cancer-associated cachexia. *Nat Rev Dis Primers*. 2018;4:17105.
41. Sambasivan R, et al. Pax7-expressing satellite cells are indispensable for adult skeletal muscle regeneration. *Development*. 2011;138(17):3647–3656.
42. Pannérec A, Marazzi G, Sassoon D. Stem cells in the hood: the skeletal muscle niche. *Trends Mol Med*. 2012;18(10):599–606.
43. Wang YX, Rudnicki MA. Satellite cells, the engines of muscle repair. *Nat Rev Mol Cell Biol*. 2012;13(2):127–133.
44. Jones NC, et al. The p38alpha/beta MAPK functions as a molecular switch to activate the quiescent satellite cell. *J Cell Biol*. 2005;169(1):105–116.
45. Hawke TJ, Garry DJ. Myogenic satellite cells: physiology to molecular biology. *J Appl Physiol*. 2001;91(2):534–551.
46. Taipaleenmäki H, et al. Targeting of Runx2 by miR-135 and miR-203 impairs progression of breast cancer and metastatic bone disease. *Cancer Res*. 2015;75(7):1433–1444.
47. Bouxsein ML, Boyd SK, Christiansen BA, Guldberg RE, Jepsen KJ, Müller R. Guidelines for assessment of bone microstructure in rodents using micro-computed tomography. *J Bone Miner Res*. 2010;25(7):1468–1486.
48. Bonetto A, Andersson DC, Waning DL. Assessment of muscle mass and strength in mice. *Bonekey Rep*. 2015;4:732.
49. Dempster DW, et al. Standardized nomenclature, symbols, and units for bone histomorphometry: a 2012 update of the report of the ASBMR Histomorphometry Nomenclature Committee. *J Bone Miner Res*. 2013;28(1):2–17.